Chemistry of Diruthenium Analogue of Pentaborane(9) With Heterocumulenes: Toward Novel Trimetallic Cubane-Type Clusters

ARTICLE *in* INORGANIC CHEMISTRY · SEPTEMBER 2014

Impact Factor: 4.76 · DOI: 10.1021/ic501623f · Source: PubMed

7 AUTHORS, INCLUDING:

R. S. Anju
Indian Institute of Technology Madras
20 PUBLICATIONS **96** CITATIONS
SEE PROFILE

Koushik Saha
Indian Institute of Technology
9 PUBLICATIONS **15** CITATIONS
SEE PROFILE

Bijan Mondal
Indian Institute of Technology Madras
34 PUBLICATIONS **143** CITATIONS
SEE PROFILE

Inorganic Chemistry

Article

pubs.acs.org/IC

Chemistry of Diruthenium Analogue of Pentaborane(9) With Heterocumulenes: Toward Novel Trimetallic Cubane-Type Clusters

R. S. Anju,[†] Koushik Saha,[†] Bijan Mondal,[†] Vincent Dorcet,[‡] Thierry Roisnel,[‡] Jean-Francois Halet,[‡] and Sundargopal Ghosh*,[†]

[†]Department of Chemistry, Indian Institute of Technology Madras, Chennai 600 036, India

[‡]Institut des Sciences Chimiques de Rennes, UMR 6226 CNRS-Université de Rennes 1, France

Supporting Information

ABSTRACT: Reactions of the CS_2 and CO_2 heterocumulene ligands with *nido*-ruthenaborane cluster $[1,2\text{-}(Cp^*Ru)_2(\mu\text{-}H)_2B_3H_7]$, **1**, were explored ($Cp^*$ = pentamethylcyclopentadienyl). Compound **1** when treated with CS_2 underwent metal-assisted hydroboration to yield *arachno*-ruthenaborane $[(Cp^*Ru)_2(B_3H_8)(CS_2H)]$, **2**, with a dithioformato ligand attached to it. The chemistry of **2** was then explored with various transition metal carbonyl compounds under photolytic and thermolytic conditions. Thermolysis of **2** with $[Mn_2(CO)_{10}]$ resulted in the formation of an unprecedented cubane-type cluster $[(Cp^*Ru)_2Mn(CO)_3(CS_2H_2)B_3H_4]$, **3**, with a rare $[M_3E_5]$ formulation (E = B, S). On the other hand, when compound **2** was photolyzed in the presence of $[Mn_2(CO)_{10}]$, it yielded an incomplete cubane-type cluster $[(Cp^*Ru)_2Mn(CO)_3BH_2(CS_2H_2)]$, **4**. The room-temperature reaction of **2** with $[Fe_2(CO)_9]$ yielded heterometallic arachno clusters $[(Cp^*Ru)(CO)_2\{Fe(CO)_3\}_2S_2CH_3]$, **6** and $[(Cp^*Ru)_2(B_3H_8)(CO)\{Fe(CO)_3\}_2(CS_2H)]$, **7**. In contrast, photolysis of **2** with $[Fe_2(CO)_9]$ yielded a tetrahedral cluster $[(Cp^*Ru)(CO)_2S(\mu\text{-}H)\{Fe(CO)_3\}_3]$, **8**, tethered to an exo-polyhedral moiety $[(Cp^*Ru)(CO)_2]$. Compound **6** provides an unusual bonding pattern by means of fusing the wing-tip vertex (S) of the $[Fe_2S_2]$ butterfly core by an exo-polyhedral $[(Cp^*Ru)(CO)_2]$ unit. Density functional theory calculations were carried out to provide insight into the mechanistic pathway, electronic structure, and bonding properties.

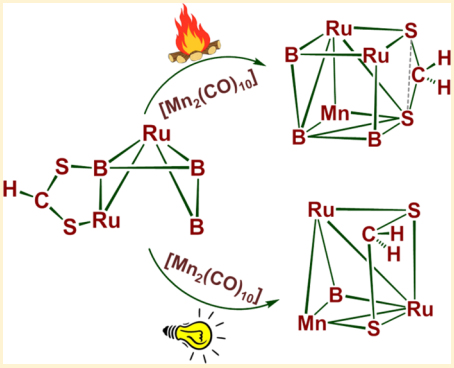

INTRODUCTION

The heterocumulene ligands such as carbonyl sulfide (COS), carbon disulfide (CS_2), and carbon dioxide (CO_2) interact with transition metal complexes showing a wide range of chemical transformations, for example, insertion, dimerization, disproportionation, coupling, and catalytic reactions.[1−3] Being a potential source of C_1-chemistry, investigations of the chemistry and bonding of these unsaturated electrophiles have triggered enormous research activities over the past few decades.[1−5] On the basis of the general concern of the electron donating/accepting properties of CS_2 and CO_2, various binding modes with one or more metal atoms have been recognized (Chart 1). For example, in the titanium-CS_2 complex, $[Cp_2Ti(CS_2)(PMe_3)]$, ($Cp = \eta^5\text{-}C_5H_5$) the CS_2 ligand exhibits a η^2-coordination mode, where a π back donation can be observed from the titanium center to the CS_2 ligand.[6] A number of bimetallic complexes such as $[Cp(CO)_2FeC(SMe)SM'L_n]$, (where $M'L_n$ = $[CpFe(CO)_2]$, $[Cr(CO)_5]$, $[Mn(CO)_5]$, $[Re(CO)_5]$, or $[W(CO)_5]$) are known in literature, in which CS_2 acts as a bridging ligand between two metal centers.[6,7] Apart from this conventional coordination chemistry, insertion of CS_2 into metal−alkyl and metal−hydride bonds to yield dithiocarboxylate or dithioformate complexes have been well documented.[6] Unlike CS_2, the isostructural CO_2 reacts with organometallic complexes in a slightly different way with

Chart 1. Various Coordination Modes of CS_2 and CO_2 with Transition Metals

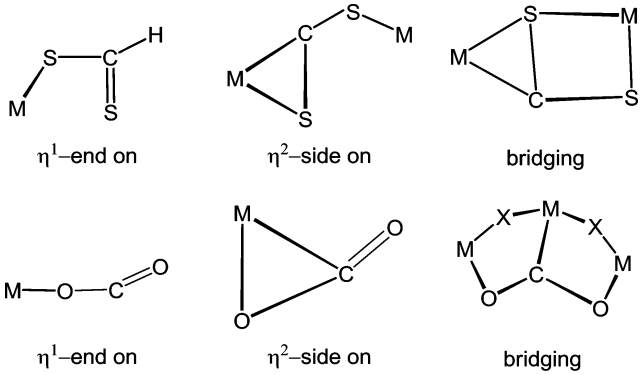

η^1-end on, η^1-C, η^2-side on, and bridging coordination modes (Chart 1).[8] The reduction of CO_2 catalyzed by transition metal complexes has also been reported.[6,9]

Although the chemistry of heterocumulenes with organometallic complexes have been studied extensively, their

Received: July 8, 2014
Published: September 25, 2014

   dx.doi.org/10.1021/ic501623f | Inorg. Chem. 2014, 53, 10527−10535

reactivity toward polyhedral metallaborane clusters remained a sparsely explored area.[10,11] Metallaborane compounds that are associated with a redox-flexible transition metal center with an electronically flexible "boron-frame" may permit interesting chemical impact on these unsaturated species. Earlier, Fehlner and co-workers described the reactivity of CS_2 with the unsaturated chromaborane cluster $[(Cp^*Cr)_2B_4H_8]$, ($Cp^* = \eta^5$-C_5Me_5), which underwent metal-assisted hydroboration and successively converted to methanedithiolato ligand.[11] With this background, we performed the reactivity of heterocumulenes with *nido*-$[1,2\text{-}(Cp^*Ru)_2(\mu\text{-}H)_2B_3H_7]$,[12] **1**. In this report, we describe the reaction of CS_2 with **1** and its subsequent transformation into $[(Cp^*Ru)_2(B_3H_8)(CS_2H)]$, **2**, which has a dithioformato ligand (CHS_2). In addition, the chemistry of **2** was explored with various transition metal carbonyl compounds under thermal and photolytic conditions that generated novel trimetallic cubane-type clusters, which are described.

RESULTS AND DISCUSSION

Reactivity of *nido*-$[1,2\text{-}(Cp^*Ru)_2(\mu\text{-}H)_2B_3H_7]$, 1, with CS_2 and CO_2. As shown in Scheme 1, compound **1** reacts

Scheme 1. Reaction of Ruthenaborane 1 with CS_2

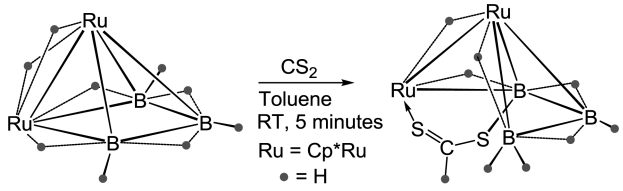

cleanly with CS_2 at room temperature to form a single product, $[(Cp^*Ru)_2(B_3H_8)(CS_2H)]$, **2**, in quantitative yield. Compound **2** was isolated as a purple solid and characterized by mass spectrometry, IR, NMR, and a single-crystal X-ray diffraction analysis. The room-temperature ^{11}B NMR spectrum of compound **2** rationalizes the presence of three boron environments, which appeared at δ = 35.6, −3.1, and −13.0 ppm in a 1:1:1 ratio. Besides the BH terminal protons, two B−H−B, two Ru−H−B, and one Ru−H−Ru protons were observed in the ^1H NMR spectrum. Furthermore, ^1H and ^{13}C NMR spectra imply two equivalent Cp* ligands.

Confirmation of the identity of **2** was made on the basis of a solid-state X-ray crystal structure. As shown in Figure 1, its molecular structure can be viewed as a diruthenium analogue of pentaborane(11) with a dithioformato ligand attached to it. The core structure of **2** can be predicted by electron counting rules,[13] to be a five-vertex, eight-skeletal-electron-pair (sep) open square pyramidal arachno cluster, very similar to that of $[1,2\text{-}\{Cp^*Ru\}_2(CO)_2B_3H_7]$.[14] A dithioformato moiety in **2**, which appears to have originated from the added CS_2 molecule, is attached to a $[(Cp^*Ru)_2B_3H_8]$ fragment, forming a five-membered {Ru−S−C−S−B} metalloheterocycle such that one sulfur atom is bonded to boron and the other is bonded to basal ruthenium atom. The formation of *arachno*-**2** from the square pyramidal *nido*-**1** might be via the coordination of CS_2 to the ruthenaborane cluster followed by the breaking of one of the Ru−B bonds. Compound **1** possesses several potentially active B−H and Ru−H−B hydrogens. As a result, it reacts instantaneously with CS_2 delivering one reducing equivalent to the bound substrate allowing metal-assisted hydroboration and partial reduction reaction. Thus, **2** can formally be

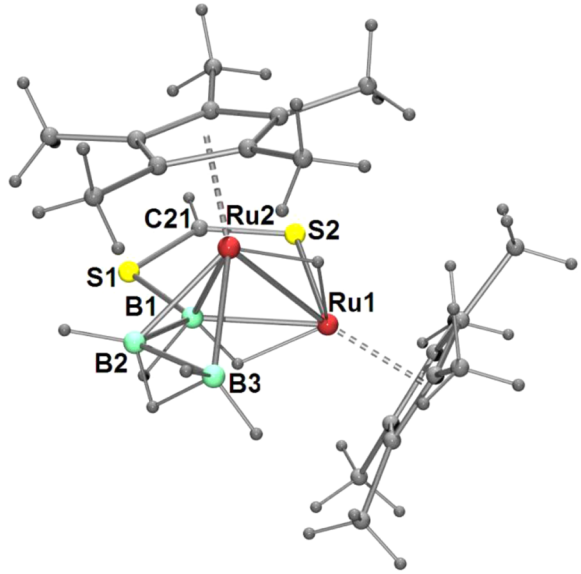

Figure 1. Molecular structure and labeling diagram of **2**. Selected bond lengths (Å) and angles (deg): B1−B2 1.803(5), B1−S1 1.904(4), B1−Ru2 2.156(3), B1−Ru1 2.266(3), B2−B3 1.872(8), B2−Ru2 2.129(4), C21−S1 1.668(4), C21−S2 1.651(4), B3−Ru2 2.278(4), S2−Ru1 2.2609(7), Ru1−Ru2 2.9738(3); B2−B1−S1 114.0(2), B2−B1−Ru2 64.35(18), S1−B1−Ru2 122.38(15), Ru2−B1−Ru1 84.50(11), B2−B1−Ru1 129.1(2), S1−B1−Ru1 116.64(16), S2−C21−S1 125.4(2).

generated from **1** by the cleavage of one Ru−B bond and subsequent reduction of the CS_2 ligand.

The structures of **1** and **2** differ both qualitatively and quantitatively. In **2**, the interatomic distance between Ru1 and Ru2 (2.9738(3) Å) is in the larger limit of reported Ru−Ru single bonds.[14] The dihedral angle between the three-membered rings of Ru2−Ru1−B1 and B2−Ru2−B1 is 138.5°, which is wider than the corresponding angle observed in *arachno*-B_4H_{10} (125.5°: electron diffraction; 117.4°: electron diffraction and microwave spectroscopy;[15] 128.4° (average (av)): *arachno*-dimetallaboranes[16]).

Encouraged by the X-ray structure of **2**, we sought to establish the reactivity pattern of **1** with other heterocumulenes, in particular, CO_2. Although CO_2 is structurally very similar to CS_2, its reactivity toward **1** is different. While CS_2 reacted with compound **1** instantaneously, the reaction with CO_2 remained inert even after heating at 60 °C for several hours, and reaction for longer time led to the decomposition of **1**. The dissimilarity in reactivity between CS_2 and CO_2 is interesting. Although one can assume this dissimilarity based on the ionization potential and electron affinity values of CS_2 and CO_2,[6] theoretical studies based on density functional theory (DFT) were performed to shed further light on this account.[17,18] Compound **1** reacts cleanly with CS_2 to form a single product, **2**. This process is exothermic (−28.96 kcal mol^{-1}) and quite exergonic (−20.43 kcal mol^{-1}). CO_2, on the other hand, remained inert even in forcing conditions as the reaction is less exothermic (−5.15 kcal mol^{-1}) and only slightly exergonic (−3.09 kcal mol^{-1}). This is in agreement with our experimental observations. From the geometrical comparison between **1** and **2**, it is understood that reaction starts with the facile addition of CS_2 ligand to metal site and is followed by metal-assisted hydroboration on C−S bond.

DFT calculations reproduce satisfactorily the experimental geometries (Table S1, Supporting Information) and ^{11}B

dx.doi.org/10.1021/ic501623f | Inorg. Chem. 2014, 53, 10527−10535

chemical shifts (Table S2, Supporting Information). The natural bond order (NBO) analysis shows that the Ru−Ru bonding strength reduces compared to **1** (Wiberg bond index (WBI): 0.31 for **1** and 0.26 for **2**), which can be explained on the basis of the number of bridging hydrogen(s) (Ru−H−Ru) present (two for **1** and one for **2**; which is known to pull the metals closer) as well as a slight effect of S atom coordinated to basal Ru atom (Table S3, Supporting Information). Figure S1 (Supporting Information) shows localized molecular orbitals (LMOs) of dithioformato ligand in **2**. Electron delocalization from atom S1 to C21−S2 and S1 to B1 was observed from NBO second-order perturbation energy analysis, which in turn may strengthen the B1−S1 bond (high WBI value of 0.97).

Reactivity of 2 toward Transition Metal Carbonyl Compounds. The reactions of transition metal fragment sources with polynuclear cluster compounds are one of the most successful ways to attain metal fragment substitutions or additions.[19−21] There has been much interest in such heterometallic transition metal clusters since they can be a possible source for many novel classes of homogeneous catalysts. As part of our current research program in the synthesis and reactivity of early and late transition metal-laborane clusters, we have been successful in developing high-yield synthetic routes to many metallaboranes, and as a result, the reactivity of metallaboranes toward metal carbonyls has been explored in detail.[22−25] For example, we have recently reported an *arachno*-ruthenaborane, $[(Cp^*Ru)_2(CO)_2(B_2H_6)]$,[23] which acted as a potential precursor for several triply bridged heterotrinuclear borylene compounds when treated with $[Fe_2(CO)_9]$.[23] Also, the DFT molecular orbital study of **1** and **2** further shows that the lowest unoccupied molecular orbital (LUMO) of **2** is significantly stabilized due to the decrease in the Ru−Ru antibonding interaction and a strong contribution of S atom of CS_2 ligand, suggesting a high degree of reactivity for **2** (Figure S2, Table S3 and S4, Supporting Information). Therefore, we carried out the reactions of **2** with metal carbonyl compounds both under thermolytic and photolytic conditions.

(I). Reactivity of 2 with $[Mn_2(CO)_{10}]$. (a). Under Thermolytic Condition. Thermolysis of **2** with $[Mn_2(CO)_{10}]$ yielded $[(Cp^*Ru)_2Mn(CO)_3(CS_2H_2)B_3H_4]$, **3**, in 40% yield. The ^{11}B NMR spectrum of **3** shows three distinct chemical shifts appearing at δ = 51.3, 46.1, and 13.7 ppm. The ^1H and ^{13}C NMR spectra indicate 2 equiv of Cp* moieties. Furthermore, the ^1H NMR spectrum shows a sharp signal at δ = −24.9 ppm corresponding to a Ru−H proton. The presence of CO ligand was confirmed by IR and ^{13}C NMR spectroscopy. An unambiguous explanation eluded us until an X−ray structure study revealed the geometry of **3** (Figure 2). The single crystals suitable for X-ray diffraction were obtained from a solution of **3** in hexane at −5 °C, allowing for the structural characterization.

The solid-state structure of **3** shows that the CHS_2 unit underwent complete reduction to generate a methanedithiolato ligand $[CH_2S_2]$ (the LMOs of CH_2S_2 ligand are shown in Figure S3, Supporting Information). The Ru1−Ru2 distance in **3** (2.7738(3) Å) is shorter, compared to both **1** and **2**. The Mn−B distances vary from 2.086(3) to 2.373(4) Å. In **3**, both C−S bonds of the methanedithiolato bridge are significantly elongated (av C−S distance 1.8185 Å) when compared to **2**, and they are in the range of a C−S single bond.[26] While one sulfur atom acts as a bridge between two Ru atoms, the other one is linked to one boron and one manganese atom resulting

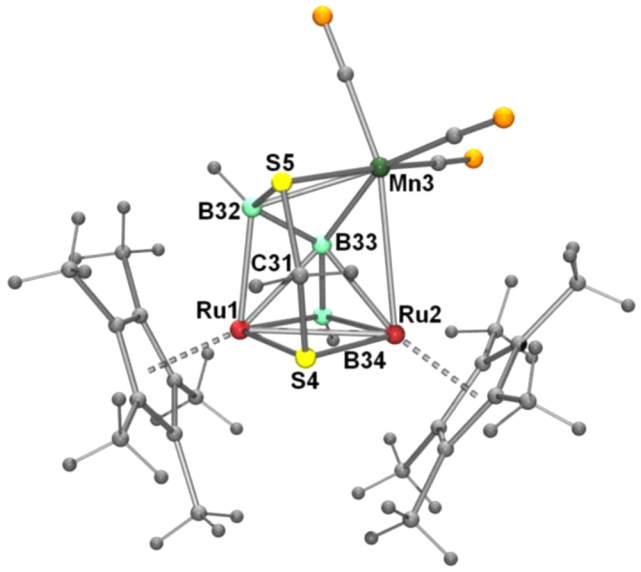

Figure 2. Molecular structure and labeling diagram of **3**. Selected bond lengths (Å) and angles (deg): Ru1−B33 2.173(3), Ru1−B32 2.244(4), Ru1−Ru2 2.7738(3), Ru2−B33 2.201(3), Mn3−B33 2.086(3), Mn3−B32 2.373(4), Mn3−S5 2.3388(8), S4−C31 1.834(3), S5−C31 1.803(3); Ru1−B32−Mn3 113.63(14), Mn3−B33−Ru2 88.80(12), Ru1−B33−Ru2 78.70(9), S5−C31−S4 114.18(16), S5−B32−Mn3 65.48(11), S5−B32−Ru1 116.27(17), B33−B32−S5 114.8(2).

in two unique five-membered metalloheterocycles [Ru1−S4−C31−S5−B32] and [Ru2−S4−C31−S5−Mn3].

The structure of **3** can be projected in two different ways: first, by assuming the sulfur atoms as the vertices of the cluster and second, by considering the CH_2S_2 fragment as a ligand that donates six electrons to the cluster. In the first approach, compound **3** displays a heterometallic cuboidal $Ru_2MnS_2B_3$ cage. When CH_2S_2 is considered as a ligand, compound **3** can be seen as a boron-capped (B34 in Figure 2) Ru_2MnB_2 nido-square pyramid (Ru1, Ru2, Mn3, B32, and B33 in Figure 2), with the CH_2S_2 ligand pending below the square face. In **3**, the interatomic separation between two sulfur atoms (3.053 Å) is significantly too long to form a direct S−S bond. A similar situation is observed in Fe−S cubane-type clusters **I**−**III**,[27] (Chart 2), where, Fe−S−S bridge/bridges is/are present. However, the presence of a bridging CH_2 group that links the far-flung vertices of the cubane core in **3** is unprecedented.

The cubane-type metal-sulfido clusters have been extensively investigated.[31] Although the shapes of all the cubane structures are qualitatively the same, the number of M−M bonds may differ depending on the cluster electron count.[21,28] The stable cluster valence electron count for an M_3E_5 cubane is 70, which is the count predicted for conventional localized 2-center-2-electron bonding. Each successive two-electron loss is generally accompanied by the formation of one M−M, M−E, or E−E bond along some diagonal of the cube.[29] With four bonds along the diagonals, (Figure 2 and Scheme 2) a count of 58 electrons is expected for **3**, which is the same as the actual experimentally observed one. A substantial HOMO−LUMO gap of 1.84 eV is computed for **3′** (Cp analogue of **3**) with such an electron count. To the best of our knowledge, compound **3** is the second entry to the rare class of structurally characterized examples of a trimetallic cubane-type cluster.[30]

(b). Under Photolytic Condition. Photolysis of compound **2** with $[Mn_2(CO)_{10}]$ in THF, followed by chromatographic

dx.doi.org/10.1021/ic501623f | *Inorg. Chem.* 2014, 53, 10527−10535

Chart 2. Cubane-Type Clusters with Bridging Atom between Two Vertices[a]

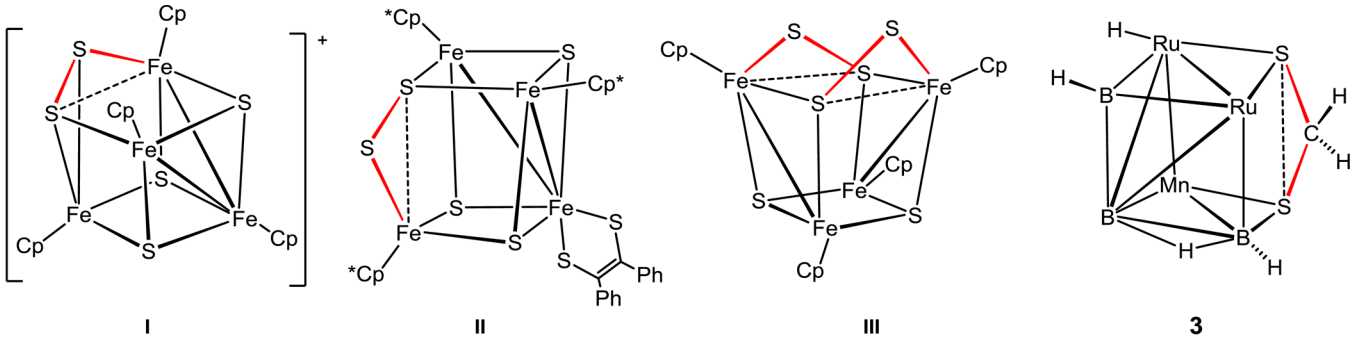

[a]Dotted lines represent the missing bonds.

Scheme 2. Reactivity of Compound 2 with $[Fe_2(CO)_9]$ (left) and $[Mn_2(CO)_{10}]$ (right)

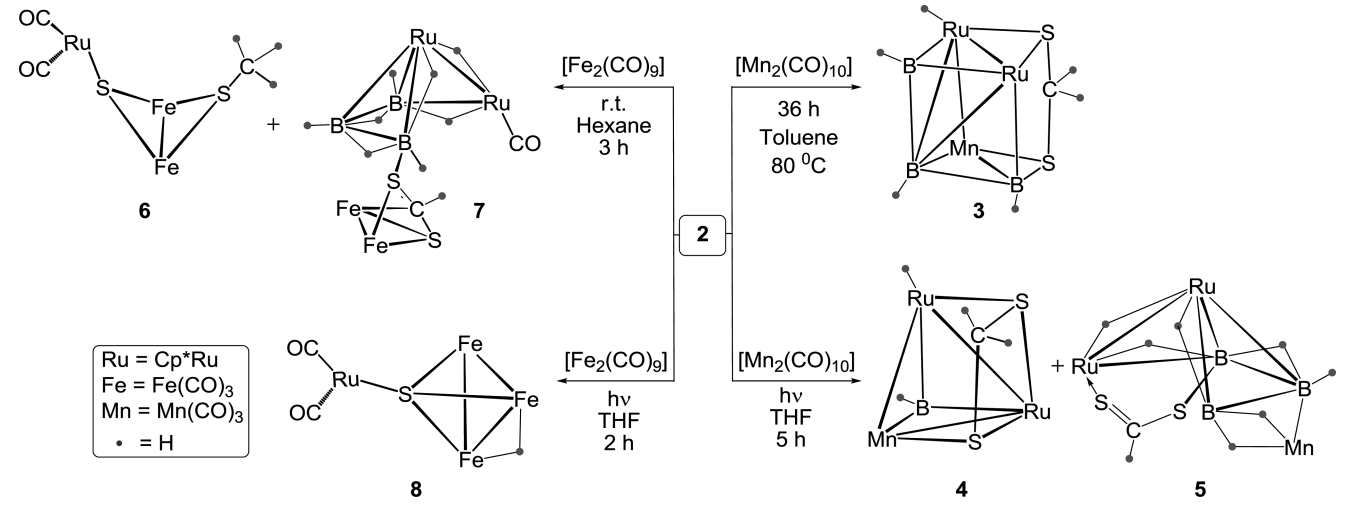

workup, led to the isolation of $[(Cp^*Ru)_2Mn(CO)_3BH_2(CS_2H_2)]$, **4** and $[(Cp^*Ru)_2Mn(CO)_3B_3H_7(CS_2H)]$, **5**, in moderate yields. The ^{11}B NMR spectrum of **4** displays a downfield chemical shift at $\delta = 126$ ppm. The ^1H NMR shows a broad resonance at $\delta = 9.9$ ppm, which is characteristic of a B−H proton of a triply bridged borylene ligand. The signals corresponding to two equivalent Cp* ligands and a terminal Ru−H proton were also observed in the ^1H NMR spectrum. A perspective view of **4**, shown in Figure 3, confirms the presence of a CH_2S_2 unit that acts as a bridging ligand between Ru and Mn atoms. The Ru1−Ru2 bond distance in **4** has been reduced by 0.2 Å when compared to that of **2**. The Mn−B, Ru−B, and C−S bond distances are in the range of a normal single bond.[22c,23,26]

The geometry of **4** can also be described as an incomplete cubane-type M_3S_2CB cage, when the carbon and sulfur atoms of the methanedithiolate group are considered as vertices. The cluster valence electron count for compound **4** is 54. This is two electrons shorter than expected, considering that an M_3E_4 "regular" cubane-like cluster is generally stable for a count of 68.[20a] Indeed, for **4**, a count of 56 should be observed since there are three M−M bonds along the diagonals of the "cube." This unsaturation might be due the presence of the triply bridged borylene unit as one of the vertices. An energy gap of 1.37 eV separates the HOMO from the LUMO in **4′**, (Cp analogue of **4**), indicating the stability for such a cluster with two electrons less than expected. Though it is difficult to amount the incomplete cubane-type clusters,[31] the ones with a triply bridged borylene unit occupying a vertex is unique.

Alternatively, compound **4** can be considered as a tetrahedral Ru_2MnB cluster, where the CH_2S_2 fragment is emphasized as a ligand. A count of cluster valence electrons of 50 (13 (Cp*Ru) × 2 + 13 ($Mn(CO)_3$) + 4 (BH) + 1 (H) + 6 (CH_2S_2)) or six sep is obtained as expected for an M_3E tetrahedral cluster. The core geometry of **4** is analogous to that observed for the isoelectronic triply bridged borylene complex $[(Cp^*RuCO)_2Mn(CO)_3BH(CO)(\mu\text{-}H)]$.[23] Figure S4 (Supporting Information) shows the triply bridged bonding situation of BH. A comparative DFT-MO study of **4** and $[(Cp^*RuCO)_2Mn(CO)_3BH(CO)(\mu\text{-}H)]$ shows that the introduction of π-donor chalcogen atoms into **4** diminishes the HOMO−LUMO gap (1.37 eV for **4′** (Cp analogue of **4**) as said before and 2.0 eV for the later).

Compound **5**, which was isolated as the major product, maintains the core structure (Figure S13, Supporting Information) of the parent molecule **2** to form an eight-sep *arachno*-pentaborane(11) metal analogue with a manganese carbonyl fragment anchored to it in η^2-fashion.[32] However, a significant variation can be observed in the B7−Mn1 and B8−Mn1 interatomic distances from 1.913 to 2.355 Å. This could be due to the presence of two bridging hydrogen atoms present between B7 and Mn.

(II). Reactivity of **2** *with* $[Fe_2(CO)_9]$. *(a). Room Temperature.* As shown in Scheme 2, the room-temperature reaction of **2** with $[Fe_2(CO)_9]$ in hexane led to the isolation of two

dx.doi.org/10.1021/ic501623f | Inorg. Chem. 2014, 53, 10527−10535

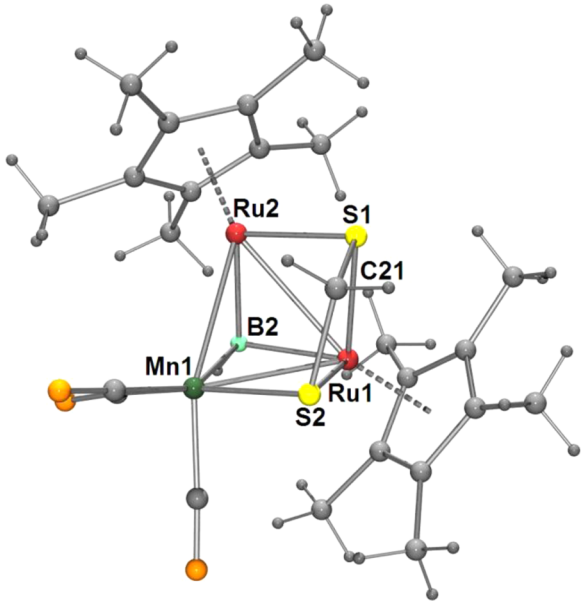

Figure 3. Molecular structure and labeling diagram of **4**. Selected bond lengths (Å) and angles (deg): B2−Ru2 2.076(10), B2−Ru1 2.081(11), B2−Mn1 2.179(10), S1−Ru2 2.287(3), S1−Ru1 2.333(2), Mn1−Ru1 2.7290(14), Mn1−Ru2 2.7973(14), Ru1−Ru2 2.7835(11), C21−S2 1.804(12), C21−S1 1.840(12), S2−Ru1 2.395(3), S2−Mn1 2.271(3); Ru2−B2−Ru1 84.1(4), Ru2−B2−Mn1 82.2(3), Ru1−B2−Mn1 79.6(4), Ru2−S1−Ru1 74.10(7), B2−Mn1−S2 104.5(3), S2−C21−S1 102.7(6).

exopolyhedral heterometallic clusters, analyzed as $[(Cp^*Ru)(CO)_2\{Fe(CO)_3\}_2S_2CH_3]$, **6** and $[(Cp^*Ru)_2(B_3H_8)(CO)\{Fe(CO)_3\}_2(HCS_2)]$, **7**. In parallel, the reaction also yielded triply bridged borylene complexes $[(\mu_3\text{-BH})(Cp^*RuCO)_2(\mu\text{-CO})\{Fe(CO)_3\}]$, $[\{(\mu_3\text{-BH})(Cp^*Ru)(\mu\text{-CO})\}_2Fe_2(CO)_5]$, and $[\{(\mu_3\text{-BH})(Cp^*Ru)Fe(CO)_3\}_2(\mu\text{-CO})]$ in low yields.[23]

Compound **6** was isolated as an orange, air-stable solid. The mass spectrometric data suggest a molecular formula of $[(Cp^*Ru)(CO)_2\{Fe(CO)_3\}_2S_2CH_3]$. Consistent with this observation, the ^1H and ^{13}C NMR spectra also showed a single Cp* resonance. The IR spectrum exhibited CO stretching frequencies at 1945 and 1979 cm^{-1}. To confirm the spectroscopic assignments and to determine the full molecular and crystal structure of **6**, an X-ray analysis was undertaken. The crystal structure of **6** corresponds to discrete molecules of $[Cp^*Ru(CO)_2Fe_2(CO)_6(\mu_3\text{-S})(\mu\text{-SCH}_3)]$ separated by normal van der Waals distances (Figure 4a). It shows an exo-polyhedral fragment $\{Cp^*Ru(CO)_2\}$ anchored to a thiometalate cluster. The Ru1−S2 bond length of 2.4131(5) Å is longer compared to the normal Ru−S distance reported in other clusters and complexes.[22c] The dihedral angle between the planes Fe1−Fe2−S2 and Fe1−Fe2−S1 (100.4°) is much less than it is in other butterfly structures, indicating that the wings of the butterfly core are less flattened. One of the C−S linkages in compound **2** has been broken to form an "open" Fe_2S_2 unit. This "open" nature may give rise to distinct reactivity pattern compared to some of the "closed" Fe_2S_2 clusters shown in Chart 3.[27] Although the geometry of the

Chart 3. "Open" and "Closed" Fe_2S_2 Cluster Types

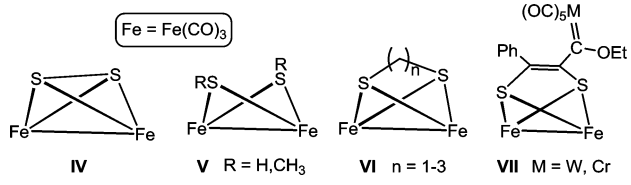

thiometalate entity in **6** is similar to the range of substituted Fe_2S_2 clusters reported in the literature,[27] there are only a very few examples of compounds with a butterfly geometry anchored to an exo-polyhedral fragment.[33]

Considering the $\{Cp^*Ru(CO)_2\}$ moiety as a one-electron fragment to the Fe_2S_2 butterfly cluster, a cluster valence electron count of 42 is achieved for compound **6** (14 $(Fe(CO)_3)$ x 2 + 7 (SMe) + 7 (S-RuCp*$(CO)_2$)) as expected. This is in agreement with a single Fe−Fe bond (2.5231(4) Å) measured experimentally. A substantial HOMO−LUMO gap of 2.2 eV is computed for **6′** (Cp analogue of **6**) with this electron count. Inspection of the electron density distribution of the

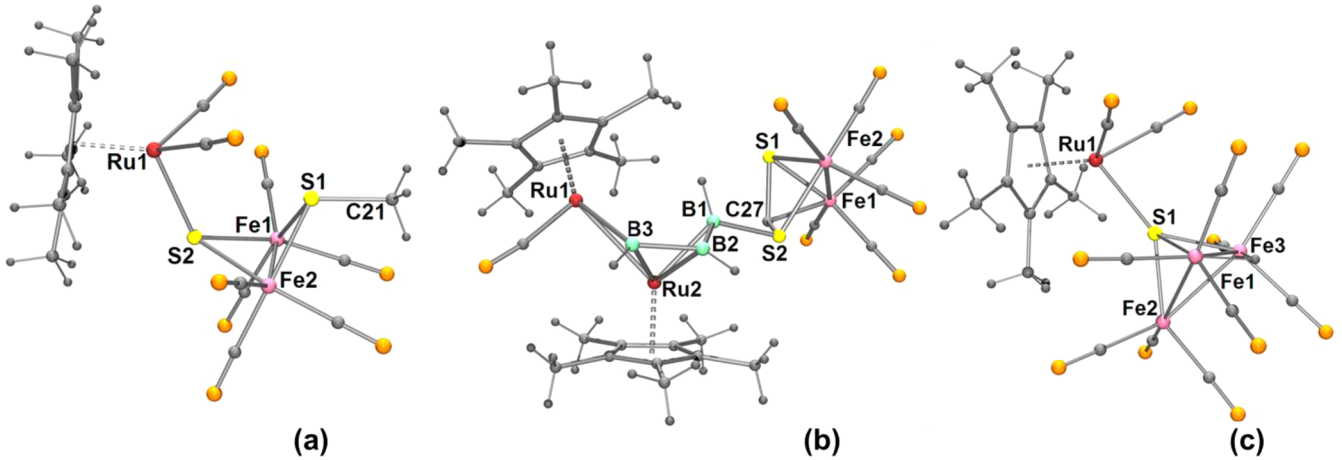

Figure 4. Selected bond lengths (Å) and angles (deg). (a) Compound **6**: S2−Ru1 2.4131(5), Fe1−S1 2.2629(6), Fe1−Fe2 2.5231(4), Fe2−S2 2.2896(6), Fe2−S1 2.2452(6) S1−C21 1.824(2); S1−Fe1−Fe2 55.635(16), S2−Fe2−Fe1 56.309(15), Fe2−S2−Ru1 123.86(2), Fe1−S2−Ru1 119.24(2). (b) Compound **7**: B1−B2 1.805(8), B1−S2 1.929(6), B1−Ru2 2.213(5), B2−B3 1.792(8), Ru1−Ru2 2.9639(5), Fe1−Fe2 2.6326(10), S1−Fe1 2.1776(17), S1−Fe2 2.2616(14), S2−Fe2 2.3301(12), C27−S1 1.784(5), C27−S2 1.795(5), C27−Fe1 2.004(5); B2−B1−S2 115.1(3), B2−B3−Ru1 122.2(3), Ru2−B3−Ru1 82.57(16), S1−C27−S2 106.8(3). (c) Compound **8**: Ru1−S1 2.4092(7), S1−Fe2−2.1727(6), S1−Fe3 2.1835(7), S1−Fe1 2.1850(6), Fe1−Fe2 2.6054(5); Fe2−S1−Fe3 73.35(2), Fe2−S1−Fe1 73.43(2), Fe2−S1−Ru1 144.08(3).

dx.doi.org/10.1021/ic501623f | *Inorg. Chem.* 2014, 53, 10527−10535

frontier molecular orbitals (FMOs, Figure S5, Supporting Information) shows that, in **6**, the HOMO is largely located on the Fe metals. Further Fe−Fe interaction was shown in HOMO−8 (WBI = 0.56). A complete bonding picture in the form of LMOs is given in Figure S6 (Supporting Information).

The ^{11}B NMR of compound **7** displayed three distinct peaks at δ = −28.7, −8.9, and −0.59 ppm. The ^{1}H NMR spectrum showed chemical shifts corresponding to B−H, B−H−B, Ru−H−B, and Ru−H−Ru protons. Its solid-state X-ray structure is consistent with the spectroscopic results. Compound **7** can be best described as a *conjuncto* cluster with an exo-polyhedral organometallic fragment [{Fe(CO)$_3$}$_2$S$_2$CH], linked to the {Ru$_2$B$_3$} *arachno* core through one of the boron atoms (Figure 4b). Out of the numerous reports available on the Hieber-type Fe−S clusters,[34a] the dominant feature of the *exo*-Fe−S fragment in **7** is the elongated Fe−Fe bond (2.6326(10) Å).[34b] The C27−S1 (1.784(5) Å) and C27−S2 (1.795(5) Å) bond distances are longer compared to those observed in **2**. It is also interesting to note that the Fe−S distances differ unusually resulting in a highly distorted square pyramidal geometry. The exo fragment may be viewed as a complex between {Fe$_2$(CO)$_6$} and a dithioformate ligand, where bonding with the Fe atom involves π electrons and the sulfur lone pair electrons of the C═S bond. A HOMO−LUMO gap of 1.8 eV is computed for **7′** (Cp analogue of **7**). Note that this cluster is isoelectronic to **2** and **5**, which adopted the same Ru$_2$B$_3$ arachno cage.

(b). Under Photolytic Condition. Compound **2**, when photolyzed in the presence of [Fe$_2$(CO)$_9$], yielded [(Cp*Ru)(CO)$_2$S(μ-H){Fe(CO)$_3$}$_3$], **8**, in which an *exo*-[(Cp*Ru)(CO)$_2$] fragment is attached to the sulfur atom (Figure 4c). The ^{1}H NMR spectrum of **8** includes resonances at 1.9 ppm assigned to the Cp* methyl protons and −21.2 ppm corresponding to a hydrido ligand. The heterometallic compound **8** displays a structure comparable to that of **6** with the count of 50 cluster valence electrons (14 (Fe(CO$_3$)) × 3 + 7 (S-RuCp*(CO)$_2$) + 1 (H)) expected for a tetrahedral M$_3$E cluster. While the Ru1−S1 and Fe−Fe distances are found to be in the normal range of single bonds, the average Fe−S bond distance in **8** (2.1805 Å) appears to be slightly shorter than in other related compounds.[26]

CONCLUSION

In this article, we have established the reactivity trends of two heterocumulene ligands, namely, CS$_2$ and CO$_2$ with a *nido*-ruthenaborane cluster. The metal-assisted hydroboration of the CS$_2$ ligand resulted in the isolation of diruthenium analogue of pentaborane(11), **2**, having a dithioformato ligand. The reactivity of **2** toward metal carbonyls such as [Mn$_2$(CO)$_{10}$] and [Fe$_2$(CO)$_9$] has been examined. The reaction with the former leads to the isolation of the first example of trimetallic cubane-type clusters, where boron is present as one of the main group constituents. In stark contrast, [Fe$_2$(CO)$_9$] shows a different reactivity pattern with **2** that gives new exo-polyhedral clusters. Investigations to evaluate the possibility of other early and late transition metal carbonyl compounds to produce complexes with rare geometries are underway, and we anticipate further progress.

EXPERIMENTAL SECTION

General Procedures and Instrumentation. All the syntheses were carried out under argon atmosphere with standard Schlenk and glovebox techniques. Solvents were dried by common methods and distilled under N$_2$ before use. Compound **1** was prepared according to literature method,[12] while other chemicals ([Cp*RuCl$_2$]$_2$, LiBH$_4$·THF, [Fe$_2$(CO)$_9$], [Mn$_2$(CO)$_{10}$], were obtained commercially and used as received. The external reference for the ^{11}B NMR, [Bu$_4$N(B$_3$H$_8$)], was synthesized according to the literature method.[35] Thin-layer chromatography (TLC) was done on 250 mm diameter aluminum-supported silica gel TLC plates (Merck TLC Plates). The NMR spectra were recorded on a 400 and 500 MHz Bruker FT-NMR spectrometer. Residual solvent protons were used as reference (δ, ppm, benzene-d_6, 7.16, CDCl$_3$, 7.26), while a sealed tube containing [Bu$_4$N(B$_3$H$_8$)] in benzene-d_6 (δ_B, ppm, −30.07) was used as an external reference for the ^{11}B NMR measurements. The infrared spectra were recorded on a Nicolet iS10 spectrometer. MALDI-TOF mass spectra of the compounds were obtained on a Bruker Ultraflextreme using 2,5-dihydroxybenzoic acid as a matrix and a ground steel target plate. The photoreactions described in this report were conducted in a Luzchem LZC-4 V photoreactor, with irradiation at 254−350 nm. Microanalyses for C and H were performed on PerkinElmer Instruments series II model 2400.

Synthesis of ***2****.* In a Flame-dried Schlenk tube, compound **1** (0.5 g, 0.97 mmol) was suspended in toluene (20 mL), and CS$_2$ (0.58 mL, 0.97 mmol) was added via syringe. The reaction mixture was stirred slowly over 5 min at room temperature. After removal of solvent, the residue was subjected to chromatographic workup using silica-gel TLC plates. Elution with hexane yielded pure purple **2** (0.56 g, 97%). **2**: MS(MALDI): m/z 589 (M$^+$), isotope envelope $C_{21}H_{39}B_3S_2Ru_2$ requires 590.2464; ^{11}B NMR (22 °C, 128 MHz, CDCl$_3$): δ = 35.6 (d, J_{B-H} = 128 Hz, 1B), −3.1 (d, J_{B-H} = 131 Hz, 1B), −13.0 (br, 1B); ^{1}H NMR (22 °C, 400 MHz, CDCl$_3$): δ = 4.8 (br, 1H, BH$_t$), 3.3 (br, 2H, BH$_t$), 3.7 (s, 1H, CH), 1.8 (s, 15H, Cp*), 1.7 (s, 15H, Cp*), −0.69 (br, 1H, B−H−B), −2.9 (br, 1H, B−H−B), −11.2(br, 1H, Ru−H−B), −15.1 (br, 1H, Ru−H−B), −15.4 (s, 1H, Ru−H−Ru); ^{13}C NMR (22 °C, 100 MHz, CDCl$_3$): δ = 101.2 (s, C_5Me_5), 103.3 (s, C_5Me_5), 36.1 (s, CH), 9.7 (s, C_5Me_5), 11.2 (s, C_5Me_5); IR (hexane, cm^{-1}): 2490 (BH$_t$), 2444 (BH$_t$), 2501 (BH$_t$); Elemental analysis calcd (%) for $C_{21}H_{39}B_3S_2Ru_2$: C, 42.73; H, 6.65; found: C, 42.44; H, 6.68.

Synthesis of ***3****.* In a flame-dried Schlenk tube, the purple solution of **2** (0.50 g, 0.84 mmol) and 2 equiv of [Mn$_2$(CO)$_{10}$] in toluene (15 mL) were thermolyzed at 80 °C for 36 h. The volatile components were removed under vacuum, and the remaining residue was passed through Celite. After removal of solvent, the residue was subjected to chromatographic workup using silica-gel TLC plates. Elution with a hexane/CH$_2$Cl$_2$ (90:10 v/v) mixture yielded brown **3** (0.24 g, 40.8%). **3**: MS(MALDI): m/z 725 [M$^+$], isotope envelope. $C_{24}H_{36}B_3O_3S_2MnRu_2$ requires 726.1819; ^{11}B NMR (22 °C, 128 MHz, CDCl$_3$): δ = 51.3 (d, J_{B-H} = 131 Hz, 1B), 46.1 (br, 1B), 13.7 (br, 1B); ^{1}H NMR (22 °C, 400 MHz, CDCl$_3$): δ = 5.9 (br, 1H, BH$_t$), 5.1 (br, 1H, BH$_t$), 4.3 (br, 1H, BH$_t$), 2.6 (s, 2H, CH$_2$), 1.8 (s, 15H, Cp*), 1.7 (s, 15H, Cp*), −24.9 (s, 1H, Ru−H); ^{13}C NMR (22 °C, 100 MHz, CDCl$_3$): δ = 188.9 (s, CO), 96.0 (s, C_5Me_5), 94.7 (s, C_5Me_5), 21.7 (s, CH$_2$), 11.5 (s, C_5Me_5), 11.1 (s, C_5Me_5); IR (hexane, cm^{-1}): 2443 (BH$_t$), 2425 (BH$_t$), 2403 (BH$_t$), 1991 (CO); Elemental analysis calcd (%) for $C_{24}H_{36}B_3O_3S_2MnRu_2$: C, 39.69; H, 4.99; found: C, 39.50; H, 4.38.

Synthesis of ***4*** *and* ***5****.* In a flame-dried Schlenk tube, a purple solution of **2** (0.50 g, 0.84 mmol) and 3 equiv of [Mn$_2$(CO)$_{10}$] in THF (15 mL) were irradiated for 5 h at room temperature. The volatile components were removed under vacuum, and the remaining residue was extracted into hexane and passed through Celite. After removal of solvent, the residue was subjected to chromatographic workup using silica-gel TLC plates. Elution with a mixture of hexane/CH$_2$Cl$_2$ (80:20 v/v) yielded green **4** (0.08 g, 13%) and red **5** (0.13 g, 21%). **4**: MS(MALDI): m/z 702 [M$^+$−H], isotope envelope. $C_{24}H_{34}BMnO_3Ru_2S_2$ requires 702.5520; ^{11}B NMR (22 °C, 128 MHz, CDCl$_3$): δ = 126.0 (d, J_{B-H} = 134 Hz, 1B); ^{1}H NMR (22 °C, 400 MHz, CDCl$_3$): δ = 9.9 (br, 1H, BH$_t$), 2.2 (s, 2H, CH$_2$), 1.8 (s, 15H, Cp*), 1.7 (s, 15H, Cp*), −19.1 (s, 1H, Ru−H); ^{13}C NMR (22 °C, 100 MHz, CDCl$_3$): δ = 192.6 (s, CO), 100.5 (s, C_5Me_5), 99.6 (s, C_5Me_5), 22.7 (s, CH$_2$), 12.2 (s, C_5Me_5), 11.6 (s, C_5Me_5); IR (hexane, cm^{-1}): 2473 (BH$_t$), 1945 (CO); Elemental analysis calcd (%) for $C_{24}H_{34}BMnO_3Ru_2S_2$: C, 41.03; H, 4.87; found: C, 41.50; H, 5.68; **5**:

dx.doi.org/10.1021/ic501623f | Inorg. Chem. 2014, 53, 10527−10535

MS(MALDI): m/z 727 [M^+], isotope envelope. $C_{24}H_{38}B_3O_3S_2MnRu_2$ requires 728.1978; ^{11}B NMR (22 °C, 128 MHz, $CDCl_3$): δ = 54.2 (br, 1B), 54.6 (br, 1B) 43.6 (s, 1B); ^{1}H NMR (22 °C, 400 MHz, $CDCl_3$): δ = 4.6 (br, 1H, BH_t), 3.4 (s, 1H, CH), 1.8 (s, 15H, Cp*), 1.7 (s, 15H, Cp*), −2.03 (br, 1H, B−H−B), −10.11 (br, 2H, Mn−H−B), −11.6(br, 1H, Ru−H−B), −14.5 (s, 1H, Ru−H−Ru), −15.5 (br,1H, B−H−Ru); ^{13}C NMR (22 °C, 100 MHz, $CDCl_3$): δ = 198.1 (s, CO), 104.2 (s, C_5Me_5), 102.8 (s, C_5Me_5), 35.8 (s, CH), 9.9 (s, C_5Me_5), 10.2 (s, C_5Me_5); IR (hexane, cm^{-1}): 2490w (BH_t), 2472 (BH_t), 2466 (BH_t), 1986 (CO); Elemental analysis calcd (%) for $C_{24}H_{38}B_3O_3S_2MnRu_2$: C, 39.58; H, 5.25; found: C, 39.33; H, 5.63.

Synthesis of ***6*** *and* ***7***. In a flame-dried Schlenk tube, the purple solution of **2** (0.50 g, 0.84 mmol) and 4 equiv of [$Fe_2(CO)_9$] in hexane (15 mL) were stirred for 2 h at room temperature. The volatile components were removed under vacuum, and the remaining residue was extracted into hexane and passed through Celite. After removal of solvent, the residue was subjected to chromatographic workup using silica-gel TLC plates. Elution with a hexane/CH_2Cl_2 (90:10 v/v) mixture yielded orange **6** (0.07 g, 12.6%) and yellow **7** (0.25 g, 37.5%). **6**: MS(MALDI): m/z 651 [M^+], isotope envelope. $C_{19}H_{18}O_8S_2Fe_2Ru$ requires 651.2367; ^{1}H NMR (22 °C, 400 MHz, $CDCl_3$): δ = 0.9 (s, 3H, CH_3), 1.7 (s, 15H, Cp*): ^{13}C NMR (22 °C, 100 MHz, $CDCl_3$): δ = 201 (s, CO), 198 (s, CO), 100.5 (s, C_5Me_5), 19.4 (s, CH_3), 12.1 (s, C_5Me_5); IR (hexane, cm^{-1}): 1945, 1979 (CO). **7**: MS(MALDI): m/z 832 [M^+], isotope envelope. $C_{28}H_{39}B_3O_7S_2Fe_2Ru_2$ requires 897.9981; ^{11}B NMR (22 °C, 128 MHz, $CDCl_3$): δ = 28.7 (br, 1B), 8.9 (d, J_{B-H} = 130 Hz, 1B), 0.5 (br, 1B); ^{1}H NMR (22 °C, 400 MHz, $CDCl_3$): δ = 5.4 (br, 1H, BH_t), 4.8 (br, 1H, BH_t), 4.1 (br, 1H, BH_t), 3.9 (s, 1H, CH), 2.0 (s, 15H, Cp*), 1.7 (s, 15H, Cp*), −1.8 (br, 1H, B−H−B), −2.0 (br, 1H, B−H−B), −11.5 (br, 1H, Ru−H−B), −12.7 (br, 1H, Ru−H−B), −17.0(s, 1H, Ru−H−Ru); ^{13}C NMR (22 °C, 100 MHz, $CDCl_3$): δ = 196.5 (s, CO), 188.3(s, CO), 187.2(s, CO), 104.2 (s, C_5Me_5), 103.5 (s, C_5Me_5), 39.3 (s, CH), 10.1 (s, C_5Me_5), 10.9 (s, C_5Me_5); IR (hexane, cm^{-1}): 2513 (BH_t), 2497 (BH_t), 2443 (BH_t), 1998 (CO), 1899 (CO); Elemental analysis calcd (%) for $C_{28}H_{39}B_3O_7S_2Fe_2Ru_2$: C, 37.44; H, 4.3775; found: C, 37.56; H, 4.30.

Synthesis of ***8***. In a flame-dried Schlenk tube, a purple solution of **2** (0.50 g, 0.84 mmol) and 2 equiv of [$Fe_2(CO)_9$] in THF (20 mL) were irradiated for 2 h at room temperature. The volatile components were removed under vacuum, and the remaining residue was extracted into hexane and passed through Celite. After removal of solvent, the residue was subjected to chromatographic workup using silica-gel TLC plates. Elution with a mixture of hexane/CH_2Cl_2 (80:20 v/v) yielded brown **8** (0.01 g, 15.8%). MS(MALDI): m/z 744 [M^+], isotope envelope. $C_{21}H_{16}O_{11}SFe_3Ru$ requires 745.0151; ^{1}H NMR (22 °C, 400 MHz, $CDCl_3$): 1.9 (s, 15H, Cp*), −20.7 (s, 1H, Fe−H−Fe); ^{13}C NMR (22 °C, 100 MHz, $CDCl_3$): δ = 188.1 (s, CO), 179.2 (s, CO), 177.5 (s, CO) 100.9 (s, C_5Me_5), 13.5 (s, C_5Me_5); IR (hexane, cm^{-1}): 1985, 1926, 1957 (CO).

X-ray Structure Determination. The crystal data for **2**−**8** were collected and integrated using an APEXII Bruker-AXS diffractometer equipped with a CCD camera and a graphite-monochromated Mo Kα (λ = 0.710 73 Å) radiation source at T = 173 K (**2**, **4**, **7**, and **8**) and 150 K (**3**, **5**, **6**). The structures were solved by heavy atom methods using SHELXS-97 or SIR92 and refined using SHELXL-97.[36,37]

Crystal Data for ***2***. $C_{21}H_{38}B_3Ru_2S_2$, M_r = 589.20, monoclinic, $P2_1/n$, a = 8.5324(4) Å, b = 13.7662(7) Å, c = 21.9638(9) Å, β = 99.7430(10)°, V = 2542.6(2) Å^3, Z = 4, F(000) = 1196, R_1 = 0.0290, wR_2 = 0.0636, 7385 independent reflections [$2\theta \leq 60.00°$] and 295 parameters.

Crystal Data for ***3***. $C_{24}H_{33}B_3MnO_3Ru_2S_2$, M_r = 723.13, monoclinic, $P2_1/n$, a = 9.8408(4) Å, b = 14.9804(7) Å, c = 19.2336(8) Å, β = 98.532(2)°, V = 2804.0(2) Å^3, Z = 4, F(000) = 1444, R_1 = 0.0413, wR_2 = 0.1034, 12220 independent reflections [$2\theta \leq 69.88°$] and 332 parameters.

Crystal Data for ***4***. $C_{24}H_{33}BMnO_3Ru_2S_2$, M_r = 701.51, monoclinic, $P2_1/n$, a = 8.6665(11) Å, b = 17.252(2) Å, c = 18.468(2) Å, β = 100.854(4)°, V = 2711.8(6) Å^3, Z = 4, F(000) = 1404, R_1 = 0. 0574, wR_2 = 0.1349, 4761 independent reflections [$2\theta \leq 50.00°$] and 421 parameters.

Crystal Data for ***5***. $C_{24}H_{38}B_3O_3S_2MnRu_2$, M_r = 728.17, orthorhombic, $P2_12_12_1$, a = 11.7260(8) Å, b = 13.8766(7) Å, c = 18.0847(11) Å, β = 90°, V = 2942.7(3) Å^3, Z = 4, F(000) = 1464, R_1 = 0.0204, wR_2 = 0.043, 6715 independent reflections [$2\theta \leq 54.90°$] and 354 parameters.

Crystal Data for ***6***. $C_{19}H_{18}Fe_2O_8RuS_2$, M_r = 651.22, monoclinic, $P2_1/n$, a = 11.1094(4) Å, b = 13.4574(4) Å, c = 16.8649(6) Å, β = 103.0930(10)°, V = 2455.82(14) Å^3, Z = 4, F(000) = 1296, R_1 = 0.0234, wR_2 = 0.0503, 5627 independent reflections [$2\theta \leq 54.94°$] and 295 parameters.

Crystal Data for ***7***. $C_{28}H_{39}B_3Fe_2O_7Ru_2S_2$, M_r = 935.02, Triclinic, $P\bar{1}$, a = 11.2880(4) Å, b = 13.4733(5) Å, c = 14.2504(5) Å, α = 78.851(2)°, β = 80.369(2)°, γ = 71.156(2)°, V = 1999.55(12) Å^3, Z = 2, F(000) = 938, R_1 = 0.0339, wR_2 = 0.0910, 7026 independent reflections [$2\theta \leq 50°$] and 446 parameters.

Crystal Data for ***8***. $C_{21}H_{16}O_{11}SFe_3Ru$, M_r = 745.02, monoclinic, $P2_1/c$, a = 9.7443(2) Å, b = 9.2221(2) Å, c = 30.2214(9) Å, β = 96.694(2)°, V = 2697.27(11) Å^3, Z = 4, F(000) = 1472, R_1 = 0.0255, wR_2 = 0.0616, 5291 independent reflections [$2\theta \leq 52°$] and 343 parameters.

Computational Details. DFT computations were carried out on simplified models **1′**−**4′** and **6′**−**7′**, that is, Cp analogues of **1**−**4** and **6**−**7** using the GAUSSIAN09 package.[17] Gas-phase geometry (no solvent effect) optimizations were carried out with the BP86 functional[38] (composed of the Becke 1988 exchange functional and the Perdew 86 correlation functional) in combination with a mixed basis set: Stuttgart/Dresden (SDD) effective core potentials (ECPs)[39] for Ru-metal center and split valence double-ς 6-31G** basis set for the remaining atoms.[40] Geometry optimizations were performed under no symmetry constraints, using initial coordinates derived from the X-ray data of the parent molecules. This level of calculation provides geometrical parameters that are in good agreement with the experimental values. Harmonic vibrational frequency calculations were done to ensure that the calculated geometries were minima on the potential energy surface (PES) and to compute zero-point energy (ZPE) corrections. Single-point calculations were also performed with the highly parametrized Zhao & Truhlar M06-2X hybrid density functional[41] and a larger combined basis set: triple-ς with diffuse functions, 6-311+G(2d,p), for C, H, O, S, and B the newly developed LANL2TZ+f basis set[42] for Ru for computing energy differences. Solvent effects were taken into account in single-point calculations on the gas-phase optimized structures using the polarizable continuum solvation model (cPCM).[43] The gauge including atomic orbital (GIAO)[44] method was used to compute the NMR chemical shifts using the hybrid Becke−Lee−Yang−Parr (B3LYP) functional[45] on the BP86/SDD-6-31g** optimized geometries. The ^{11}B NMR chemical shifts were calculated relative to B_2H_6 (B3LYP B shielding constant 94.88 ppm) and converted to the usual [BF_3·OEt_2] scale using the experimental δ(^{11}B) value of B_2H_6, 16.6 ppm.[46] The NBO[47,48] analyses were performed on the electron densities computed on the optimized geometries with the same basis sets (used for geometry optimizations), using the NBO routine within the Gaussian09 package. Molecular orbitals and vibrational modes were visualized using the GaussView program.[49]

■ ASSOCIATED CONTENT

Supporting Information

Crystallographic data in tables, images and X-ray crystallographic CIF files for **2**−**8**. This material is available free of charge via the Internet at http://pubs.acs.org.

■ AUTHOR INFORMATION

Corresponding Author

*E-mail: sghosh@iitm.ac.in.

Notes

The authors declare no competing financial interest.

■ ACKNOWLEDGMENTS

This work was supported by the Indo-French Centre for the Promotion of Advanced Research (IFCPAR-CEFIPRA), Grant No. 4405-1, New Delhi, India. R.S.A. is grateful to University Grants Commission (UGC) for fellowship; K.S. and B.M. thank IIT Madras. We thank Dr. B. Varghese, SAIF, IIT Madras, for X-ray crystallography analysis.

■ REFERENCES

(1) Pandey, K. K.; Nigam, H. L. *Rev. Inorg. Chem.* **1984**, *6*, 69−81.
(2) Ibers, J. A. *Chem. Soc. Rev.* **1982**, *11*, 57−73.
(3) (a) Choy, V. J.; O'Connor, C. J. *Coord. Chem. Rev.* **1973**, *9*, 145−170. (b) Walther, D. *Coord. Chem. Rev.* **1987**, *79*, 135−174.
(4) Baird, M. C.; Wilkinson, G. *J. Chem. Soc., Chem. Commun. (London)* **1966**, 514−515.
(5) Butler, I. S.; Fenster, A. E. *J. Organomet. Chem.* **1974**, *66*, 161−194.
(6) Pandey, K. K. *Coord. Chem. Rev.* **1995**, *140*, 37−114.
(7) Busetto, L.; Palazzi, A.; Monari, M. *J. Organomet. Chem.* **1982**, *228*, C19−C20.
(8) (a) Sakaki, S.; Kitaura, K.; Morokuma, K. *Inorg. Chem.* **1982**, *21*, 760−765. (b) Mealli, C.; Hoffmann, R.; Stockis, A. *Inorg. Chem.* **1984**, *23*, 56−65. (c) Sakaki, S.; Kitaura, K.; Morokuma, K.; Ohkubo, K. *Inorg. Chem.* **1983**, *22*, 104−108. (d) Sakaki, S.; Ohkubo, K. *Organometallics* **1989**, *8*, 2970−2973.
(9) Froehlich, H. O.; Schreer, H. *Z. Chem.* **1983**, *23*, 348−353.
(10) Coldicott, R. S.; Kennedy, J. D.; Pett, M. T. *J. Chem. Soc., Dalton Trans.* **1996**, 3819−3824.
(11) (a) Hashimoto, H.; Shang, M.; Fehlner, T. P. *Organometallics* **1996**, *15*, 1963−1965. (b) Hartwig, J. F.; Huber, S. *J. Am. Chem. Soc.* **1993**, *115*, 4908−4909. (c) Stephen, A. W.; Marder, T. B.; Baker, R. T. *Organometallics* **1993**, *12*, 975−979. (d) Evans, D. A.; Fu, G. C.; Hoveyda, A. H. *J. Am. Chem. Soc.* **1992**, *114*, 6671−6679.
(12) Lei, X.; Shang, M.; Fehlner, T. P. *J. Am. Chem. Soc.* **1999**, *121*, 1275−1287.
(13) (a) Wade, K. *Adv. Inorg. Chem. Radiochem.* **1976**, *18*, 1−66. (b) Mingos, D. M. P. *Nature (London), Phys. Sci.* **1972**, *239*, 16−26. (c) Mingos, D. M. P.; Wales, D. J. *Introduction to Cluster Chemistry;* Prentice Hall: New York, 1990.
(14) Geetharani, K.; Bose, S. K.; Sahoo, S.; Varghese, B.; Mobin, S. M.; Ghosh, S. *Inorg. Chem.* **2011**, *50*, 5824−5832.
(15) Nordman, C. E.; Lipscomb, W. N. *J. Chem. Phys.* **1953**, *21*, 1856−1864.
(16) (a) Hata, M.; Kawano, Y.; Shimoi, M. *Inorg. Chem.* **1998**, *37*, 4482−4483. (b) Anju, V. P.; Barik, S. K.; Mondal, B.; Ramkumar, V.; Ghosh, S. *ChemPlusChem* **2014**, *79*, 546−551.
(17) All calculations were done using the Gaussian 09 program by Frisch, M. J. et al. *Gaussian 09, revision C.01;* Gaussian, Inc.: Wallingford, CT, 2009. See Supporting Information for full reference.
(18) (a) Thakur, A.; Chakrahari, K. K. V.; Mondal, B.; Ghosh, S. *Inorg. Chem.* **2013**, *52*, 2262−2264. (b) Bose, S. K.; Geetharani, K.; Sahoo, S.; Reddy, K. H. K.; Varghese, B.; Jemmis, E. D.; Ghosh, S. *Inorg. Chem.* **2011**, *50*, 9414−9422.
(19) Walther, D. *Coord. Chem. Rev.* **1987**, *79*, 135−174.
(20) (a) Fehlner, T. P.; Halet, J.-F.; Saillard, J.-Y. *Molecular Clusters. A Bridge to Solid-State Chemistry;* Cambridge University Press: Cambridge, England, 2007. (b) Housecroft, C. E. In *Inorganometallic Chemistry;* Fehlner, T. P., Ed.; Plenum: New York, 1992.
(21) (a) Barton, L.; Srivastava, D. K.. Chapter 8. In *Comprehensive Organometallic Chemistry II,* Vol. *1*; Abel, E., Stone, F. G. A., Wilkinson, G., Eds.; Pergamon: New York, 1995. (b) Grimes, R. N. Chapter 9. In *Comprehensive Organometallic Chemistry II,* Vol. *1*; Abel, E., Stone, F. G. A., Wilkinson, G., Eds.; Pergamon: New York, 1995.
(22) (a) Bose, S. K.; Geetharani, K.; Varghese, B.; Mobin, S. M.; Ghosh, S. *Chem.—Eur. J.* **2008**, *14*, 9058−9064. (b) Bose, S. K.; Geetharani, K.; Ramkumar, V.; Mobin, S. M.; Ghosh, S. *Chem.—Eur. J.* **2009**, *15*, 13483−13490. (c) Anju, R. S.; Roy, D. K.; Mondal, B.; Yuvaraj, K.; Arivazhagan, C.; Saha, K.; Varghese, B.; Ghosh, S. *Angew. Chem.* **2014**, *126*, 2917−2921; *Angew. Chem., Int. Ed.* **2014**, *53*, 2873−2877.
(23) Geetharani, K.; Bose, S. K.; Varghese, B.; Ghosh, S. *Chem.—Eur. J.* **2010**, *16*, 11357−11366.
(24) (a) Dhayal, R. S.; Chakrahari, K. K. V.; Varghese, B.; Mobin, S. M.; Ghosh, S. *Inorg. Chem.* **2010**, *49*, 7741−7747. (b) Bose, S. K.; Geetharani, K.; Ramkumar, V.; Varghese, B.; Ghosh, S. *Inorg. Chem.* **2010**, *49*, 2881−2888. (c) Roy, D. K.; Bose, S. K.; Anju, R. S.; Mondal, B.; Ramkumar, V.; Ghosh, S. *Angew. Chem.* **2013**, *125*, 3304−3308; *Angew. Chem., Int. Ed.* **2013**, *52*, 3222−3226. (d) Anju, R. S.; Roy, D. K.; Geetharani, K.; Mondal, B.; Varghese, B.; Ghosh, S. *Dalton Trans.* **2013**, *42*, 12828−12831.
(25) (a) Roy, D. K.; Bose, S. K.; Geetharani, K.; Chakrahari, K. K. V.; Mobin, S. M.; Ghosh, S. *Chem.—Eur. J.* **2012**, *18*, 9983−9991. (b) Geetharani, K.; Bose, S. K.; Sahoo, S.; Ghosh, S. *Angew. Chem.* **2011**, *123*, 3994−3997; *Angew. Chem., Int. Ed.* **2011**, *50*, 3908−3911.
(26) Raubenheimer, H. G.; Linford, L.; Lombard, A. V. A. *Organometallics* **1989**, *8*, 2062−2063.
(27) Ogino, H.; Inomata, S.; Tobita, H. *Chem. Rev.* **1998**, *98*, 2093−2121.
(28) Kennedy, J. D. *Prog. Inorg. Chem.* **1984**, *34*, 211−434.
(29) Stark, J. L.; Harms, B.; Guzmann-Jimenez, I.; Whitmire, K. H.; Gautier, R.; Halet, J.-F.; Saillard, J.-Y. *J. Am. Chem. Soc.* **1999**, *121*, 4409−4418.
(30) Eveland, J. R.; Whitmire, K. H. *Angew. Chem.* **1997**, *109*, 1241−1242; *Angew. Chem., Int. Ed. Engl.* **1997**, *36*, 1193−1194.
(31) (a) Oya, K.; Seino, H.; Akiizumi, M.; Mizobe, Y. *Organometallics* **2011**, *30*, 2939−2946. (b) Miguel, D.; Riera, V.; Wang, M.; Bois, C.; Halut, S. *Inorg. Chem.* **1998**, *37*, 5944−5947.
(32) The formation of compound **5** can be justified on the basis of isolobal analogy. Replacement of a hydrogen atom in compound **2** by an isolobal $\{Mn(CO)_3\}$ fragment generated compound **5** in 21% yield as a red solid.
(33) Alvarez, B.; Alvarez, M. A.; Amor, I.; García, M. E.; Ruiz, M. A. *Inorg. Chem.* **2011**, *50*, 10561−10563.
(34) (a) Hieber, W.; Spacu, P. *Z. Anorg. Allg. Chem.* **1937**, *233*, 353−364. (b) Shaver, A.; Fitzpatrick, P. J.; Steliou, K.; Butler, I. S. *J. Am. Chem. Soc.* **1979**, *101*, 1313−1315.
(35) Ryschkewitsch, G. E.; Nainan, K. C. *Inorg. Synth.* **1974**, *15*, 113−114.
(36) SIR92 Altornare, A.; Cascarano, G.; Giacovazzo, C.; Guagliardi, A. *J. Appl. Crystallogr.* **1993**, *26*, 343−350.
(37) (a) Sheldrick, G. M. *SHELXS-97;* University of Göttingen: Germany, 1997. (b) Sheldrick, G. M. *SHELXL-97;* University of Göttingen: Germany, 1997.
(38) (a) Schmider, H. L.; Becke, A. D. *J. Chem. Phys.* **1998**, *108*, 9624−9631. (b) Perdew, J. P. *Phys. Rev. B* **1986**, *33*, 8822−8830.
(39) Dolg, M.; Stoll, H.; Preuss, H. *Theor. Chim. Acta.* **1993**, *85*, 441−450.
(40) (a) Stephens, P. J.; Devlin, F. J.; Chabalowski, C. F.; Frisch, M. J. *J. Phys. Chem.* **1994**, *98*, 11623−11627. (b) Foresman, J. B.; Frisch, E. *Exploring Chemistry with Electronic Sructure Methods,* 2nd ed.; Gaussian, Inc.: Pittsburgh, PA, 1996.
(41) Zhao, Y.; Truhlar, D. G. *Theor. Chem. Acc.* **2008**, *120*, 215−241.
(42) (a) Roy, L. E.; Hay, P. J.; Martin, R. L. *J. Chem. Theory Comput.* **2008**, *4*, 1029−1031. (b) Ehlers, A. W.; Böhme, M.; Dapprich, S.; Gobbi, A.; Höllwarth, A.; Jonas, V.; Köhler, K. F.; Stegmann, R.; Veldkamp, A.; Frenking, G. *Chem. Phys. Lett.* **1993**, *208*, 111−114.
(43) (a) Barone, V.; Cossi, M. *J. Phys. Chem. A* **1998**, *102*, 1995−2001. (b) Cossi, M.; Rega, N.; Scalmani, G.; Barone, V. *J. Comput. Chem.* **2003**, *24*, 669−681.
(44) (a) London, F. *J. Phys. Radium* **1937**, *8*, 397−409. (b) Ditchfield, R. *Mol. Phys.* **1974**, *27*, 789−807. (c) Wolinski, K.; Hinton, J. F.; Pulay, P. *J. Am. Chem. Soc.* **1990**, *112*, 8251−8260.
(45) (a) Becke, A. D. *Phys. Rev. A* **1988**, *38*, 3098−3100. (b) Lee, C.; Yang, W.; Parr, R. G. *Phys. Rev. B* **1988**, *37*, 785−789. (c) Becke, A. D. *J. Chem. Phys.* **1993**, *98*, 5648−5652.
(46) Onak, T.; Landesman, H. L.; Williams, R.; Shapiro, I. *J. Phys. Chem.* **1959**, *63*, 1533−1535.

(47) Weinhold, F. C.; Landis, R. *Valency and bonding: A natural bond orbital donor-acceptor perspective;* Cambridge University Press: Cambridge, U.K., 2005.
(48) Reed, A. E.; Curtiss, L. A.; Weinhold, F. *Chem. Rev.* **1988**, *88*, 899−926.
(49) Dennington, R., II; Keith, T.; Millam, J.; Eppinnett, K.; Hovell, W.; Gilliland, R. *GaussView, Version 3.09;* Semichem, Inc.: Shawnee, KS, 2003.